Journal of Materials Chemistry A

ROYAL SOCIETY OF CHEMISTRY

PAPER

View Article Online
View Journal | View Issue

Check for updates

Cite this: J. Mater. Chem. A, 2019, 7, 10998

A tandem redox system with a cobalt complex and 2-azaadamantane-*N*-oxyl for fast dye regeneration and open circuit voltages exceeding 1 V†

Natalie Flores-Díaz, [a] Hee-won Bahng, [bc] Nikolaos Vlachopoulos, [a] Jacques-E. Moser, [bc] Shaik M. Zakeeruddin, *[d] Michael Grätzel [d] and Anders Hagfeldt *[a]

Received 14th January 2019
Accepted 1st April 2019

DOI: 10.1039/c9ta00490d

rsc.li/materials-a

A new tandem electrolyte composed of two redox pairs, the organic radical 2-azaadamantane-*N*-oxyl (AZ) and the well-known redox pair $[Co(bpy)_3]^{3+/2+}$ was investigated in dye sensitized solar cells. Importantly, an increase in V_{OC} was achieved using the new tandem redox system with values up to 1007 mV, compared to only 896 mV for the reference $[Co(bpy)_3]^{3+/2+}$ couple. Consequently, the tandem electrolytes presented higher device performance in conjunction with the organic dye XY1. It was determined that the V_{OC} improvement is mainly attributed to the combined effect of two factors: the more positive redox potential of the small donor AZ (0.81 V *vs.* SHE) and improved recombination resistance in the tandem electrolytes.

Introduction

The increasing global concern, about the high impact of increasing energy consumption on climate change and sustainability, focusses attention on the major challenge of this century, to migrate from a fossil fuel-based to a renewable-based energy matrix, by developing efficient and price-competitive harvesting technologies, as well as storage and proper grid management.

High-efficiency dye-sensitized solar cells (DSSCs) have drawn a lot of attention since they were first introduced in 1991.[1] They can be produced in a variety of colors and shapes and can reach energy conversion efficiencies of up to 14.3%.[2] In general, they are composed of a mesoporous colloidal semiconductor photoanode such as TiO_2 deposited on a glass substrate (usually SnO_2:F, FTO), which is then sensitized by dye molecules, a counter electrode (CE) endowed with a thin layer of an electrocatalytic material such as poly(3,4-ethylenedioxythiophene) (PEDOT), and a liquid electrolyte or a solid hole-transport material placed between these two electrodes.[3] Incoming light excites electrons from the HOMO of the dye to its excited state (approximately the LUMO level of the dye), which in turn are injected into the conduction band of the semiconductor. Subsequently they are transported through the conduction band of the semiconductor layer[4] to later exit the circuit, producing useful work, whereafter they reduce a redox mediator in the electrolyte at the CE. After electron injection, the oxidized dye is regenerated by electron transfer from the reduced form of a redox couple in the liquid electrolyte; therefore, the redox mediator in the electrolyte plays a key role to attain high energy conversion efficiencies.

The redox couple I^-/I_3^- has been widely used due to the slow recombination reaction with electrons, originating either from the semiconductor or the conductive support, resulting in high electron lifetimes;[5,6] consequently, high energy conversion efficiencies can thus be obtained.[7] Nevertheless, this redox couple has several disadvantages such as corrosiveness, absorption of light by its oxidized form in the visible range, volatility of I_2 present in solution in low concentrations in equilibrium with I^- and I_3^-, and the substantial mismatch of the redox potential of I^-/I_3^- and that of the ground state of most dyes of interest to DSSCs. The resulting high voltage loss for dye regeneration limits the device V_{OC} for I^-/I_3^- redox electrolytes to values between 0.7 and 0.8 V.[8–10]

Cobalt complexes such as $[Co(bpy)_3]^{3+/2+}$ (where bpy = 2,2′-bipyridine) have shown a rather good redox potential match with the HOMO of the dyes so that less driving force is spent for

[a]Laboratory of Photomolecular Science, Institute of Chemical Sciences & Engineering, École polytechnique fédérale de Lausanne, 1015, Lausanne, Switzerland. E-mail: anders.hagfeldt@epfl.ch

[b]Photochemical Dynamics Group, Institute of Chemical Sciences & Engineering, École polytechnique fédérale de Lausanne, 1015, Lausanne, Switzerland

[c]Lausanne Center for Ultrafast Science (LACUS), École polytechnique fédérale de Lausanne, 1015, Lausanne, Switzerland

[d]Laboratory of Photonics and Interphases, Institute of Chemical Sciences & Engineering, École polytechnique fédérale de Lausanne, 1015, Lausanne, Switzerland. E-mail: shaik.zakeer@epfl.ch

† Electronic supplementary information (ESI) available: Cyclic voltammograms of AZ and ferrocene, current density *vs.* voltage plots for symmetric cells, chronopotentiometry plots, Nyquist plots for symmetrical cells, photovoltaic parameter statistics, Nyquist plots for complete devices under dark conditions and EIS analysis, and TAS measurements. See DOI: 10.1039/c9ta00490d

Published on 02 April 2019. Downloaded by ECOLE POLYTECHNIC FED DE LAUSANNE on 5/11/2019 11:03:30 AM.

This journal is © The Royal Society of Chemistry 2019

Published on 02 April 2019. Downloaded by ECOLE POLYTECHNIC FED DE LAUSANNE on 5/11/2019 11:03:30 AM.

dye regeneration,[11–13] leading to higher open circuit voltages (V_{OC}) and higher power conversion efficiencies (η), such as 14.3% reached by the complex $[Co(phen)_3]^{3+/2+}$ with a co-sensitized organic dye (ADEKA and LEG4) photoanode.[2] Nonetheless, DSSCs using cobalt complex electrolytes normally show mass transport problems in the electrolyte due to the large size of the complexes, which also affects the dye regeneration rate, resulting in low-performing devices.[14] Another undesirable issue with these complexes is related to their absorption of light in the visible range, which although weak, compete with the dye absorption and reduce electron injection into the TiO_2 conduction band.[15] This problem can be solved by engineering of organic redox couples with low absorption in the visible range, such as disulfide/thiolate,[16] or by increasing the molar extinction coefficient of dyes compared to that of the redox complexes. Recently, the introduction of copper complexes, with high redox potentials ranging between 0.87 and 0.97 V achieving dye regeneration at low driving force of 0.1–0.2 eV, enabled V_{OC} values exceeding 1 V,[17] and PCEs of 13% and 11% for liquid electrolytes[18] and solid-state devices, respectively, the latter using copper complexes as hole transport materials.[19]

An interesting approach to further reduce the voltage loss during dye regeneration and to address diffusion problems of the redox active complexes in electrolytes is the use of so-called tandem electrolytes employing a second redox pair in the electrolyte with a more positive redox potential than that of either cobalt or copper complexes.

The organic radical (2,2,6,6-tetramethylpiperidin-1-yl)oxyl, TEMPO, with a redox potential of 0.89 V *vs.* SHE,[20–22] enhanced the performance as a tandem partner to $[Co(bpy)_3]^{3+/2+}$ compared to that of a $[Co(bpy)_3]^{3+/2+}$ alone from $\eta = 7.1\%$ to $\eta = 8.4$.[23] Another tandem based on $[Co(bpy)_3]^{3+/2+}$ and the organic electron donor tris(*p*-anisyl)amine (TPPA), the latter with $E^\circ = 0.94$ V *vs.* SHE, showed improved DSSC metrics of $V_{OC} = 920$ mV, $J_{SC} = 15.5$ mA cm^{-2}, FF = 73% and PCE = 10.5% compared to $V_{OC} = 820$ mV, $J_{SC} = 13.9$ mA cm^{-2}, FF = 72.4% and PCE = 8.3% for the reference without TPPA.[24]

By judicious selection of a TEMPO derivative we aimed to increase the stability of the $TEMPO^+$ cation in the electrolyte and increase the V_{OC} of the solar cells, which would lead to an increase in device performance. The organic radical 2-azaadamantane-*N*-oxyl, AZADO (abbreviated as AZ), was chosen as a donor with higher steric impediment compared to TEMPO,[25] providing higher stability to its oxidized form $AZADO^+$, as previously demonstrated by Kato *et al.*,[26] and preventing self-disproportionation by abstraction of an alpha H atom, which would lead to the formation of a double bond N=C in the ring and it is not possible due to the rigidness of the latter.[26,27] For a better understanding of the role of each species in the tandem systems, different electrolyte compositions and their action in DSSCs were studied.

Experimental methods

All chemicals and solvents were purchased from Sigma-Aldrich and TCI chemicals, if not otherwise noted, and were used without further purification.

DSSC fabrication

Glass substrates with fluorine-doped tin oxide (FTO, NSG-10, Nippon Sheet Glass) were cleaned with 0.2% (w/w) detergent solution in an ultrasonic bath for 1 h and rinsed with water, ethanol and acetone, followed by a UV/O_3 (Model no. 256-220, Jelight Company Inc.) treatment for 15 min. The FTO substrates were immersed for 30 min in a 40 mM aqueous $TiCl_4$ solution at 70 °C to form a thin TiO_2 blocking layer and then washed with water and ethanol, followed by a sintering process at 250 °C for 2 h. Mesoporous TiO_2 films of 0.25 cm^2 were prepared by screen printing a 4.5 μm thick colloidal TiO_2 (Dyesol paste DSL 30 NRD-T) layer and drying at 120 °C in air for 5 min. If needed additional transparent colloidal TiO_2 layers were added to increase the film thickness layers by screen printing. Subsequently, a 4 μm thick light-scattering layer consisting of 400 nm sized TiO_2 particles (Dyesol WER2-0) was deposited on top by screen-printing. The films were then gradually heated in air in an oven (Nabertherm controller P320), applying a four-level program: 125 °C (10 min), 250 °C (10 min), 350 °C (10 min), and 450 °C (30 min). After sintering, the electrodes were treated in aqueous $TiCl_4$ at 70 °C for 30 min, and washed with water and ethanol. The thickness of the TiO_2 films was measured with a profilometer (Veeco Dektak 3). A final heating step at 500 °C (30 min) was performed followed by overnight immersion of the electrodes in the dye bath solution. The dye bath composition was 0.1 mM XY1 (Dyenamo AB chemicals) with 5 mM CDCA (chenodeoxycholic acid) in *tert*-butyl alcohol and acetonitrile (1 : 1). After immersion, all films were rinsed in acetonitrile to remove the excess dye. Solar cells were assembled using a 25 μm thick thermoplastic Surlyn® frame as a sealant and spacer between electrodes, with a counter electrode composed of poly(3,4-ethylenedioxythiophene) (PEDOT) deposited on NSG TEC 8™ (Pilkington) FTO-type conducting glass. The PEDOT electrodes were prepared by electropolymerization of 3,4-ethylenedioxythiophene (EDOT) from a micellar aqueous solution of 0.1 M sodium *n*-dodecyl sulfate (SDS) and 0.01 M EDOT. The electrolyte solution was introduced under vacuum through a hole predrilled in the counter electrode, which was sealed with thermoplastic Surlyn® and a glass coverslip. The electrolyte compositions were (a) the cobalt reference electrolyte: 0.22 M $Co(bpy)_3(TFSI)_2$ (bpy = 2-2′-bipyridine, TFSI = $N(CF_3SO_2)_2$) (Dyenamo AB chemicals), 0.05 M $Co(bpy)_3(TFSI)_3$ (Dyenamo AB chemicals), 0.1 M LiTFSI, and 0.5 M 4-(5-nonyl)pyridine (NP) in acetonitrile, and the tandem systems consisted of: (b) Co/AZ 1 : 1 : 0.22 M AZ, 0.22 M $Co(bpy)_3(TFSI)_2$, 0.05 M $Co(bpy)_3(TFSI)_3$, 0.1 M LiTFSI, and 0.5 M NP in acetonitrile, (c) Co/AZ 1 : 0.8 : 0.17 M AZADO, 0.22 M $Co(bpy)_3(TFSI)_2$, 0.05 M $Co(bpy)_3(TFSI)_3$, 0.1 M LiTFSI, and 0.5 M NP in acetonitrile, (d) AZ/Co 1 : 0.9 : 0.17 M AZ, 0.15 M $Co(bpy)_3(TFSI)_2$, 0.0375 M $Co(bpy)_3(TFSI)_3$, 0.1 M LiTFSI, and 0.5 M NP in acetonitrile and (e) the AZ^+/AZ^0 electrolyte: 0.25 M AZ, 0.05 M AZ^+, 0.1 M CDOA, 0.1 M LiTFSI, and 0.5 NP. In the latter electrolyte, AZ^+ is generated by addition of the oxidant 0.05 M $NOBF_4$ to an electrolyte containing 0.3 M AZ and the other components. The symmetric cells were fabricated with two PEDOT/FTO electrodes sealed together with 35 μm Surlyn® and filled with the redox electrolytes to be tested.

Published on 02 April 2019. Downloaded by ECOLE POLYTECHNIC FED DE LAUSANNE on 5/11/2019 11:03:30 AM.

Electrochemical measurements

Cyclic voltammetry measurements were performed with a potentiostat Bio Logic SP300, in a three-electrode setup cell. A glassy carbon electrode served as the working electrode (0.07 cm^2 area) and a graphite rod as the counter electrode; a non-aqueous reference electrode of Ag/AgCl (1 M LiCl in ethanol) was used, with an intermediate bridge tube containing the same supporting electrolyte as the working electrode compartment. The electrolyte solutions contained 2 mM AZ, and 0.1 M LiTFSI as the supporting electrolyte in dry acetonitrile. The scan rate was 100 mV s^{-1}, formal potentials were determined *vs.* ferrocenium/ferrocene as a reference system, and then *vs.* SHE (with a value established for $Fc^+/Fc = 0.624$ V *versus* SHE in acetonitrile and at 25 °C).[28] Cyclic voltammetry measurements to determine the current–potential plots of the symmetrical cells were also performed with the Bio Logic SP300 potentiostat. For the diffusion coefficient determination, current–voltage measurements were performed with a potentiostat/galvanostat AUT 71326 Metrohm/Autolab. A glassy carbon rotating disk electrode served as the working electrode and a graphite rod as the counter electrode; a non-aqueous reference electrode of Ag/AgCl (1 M LiCl in ethanol) was used. The electrode rotation rate was set at 1000 rpm for all the experiments.

Solar cell characterization

Current–voltage (*I–V*) characteristic curves and photocurrent-dynamics were measured using a 450 W xenon lamp (Oriel USA) as the light source, with a K113 filter Schott Tempax and matched with AM 1.5G solar standard conditions using a reference Si photodiode. The current and voltage were measured and controlled using a Keithley 2400 digital source meter (Keithley, USA) and the current measurement was set up to be delayed by 80 ms from applying the potential. A set of metal mesh filters was used to adjust the light intensity to a desired level. A black metal mask with a 0.16 cm^2 aperture was used to define the active area.

Incident photon to current efficiency, IPCE

Data were obtained using a modulated light intensity with a frequency of 1 Hz. Light from a 300 W xenon light source (ILC Technology, USA), was focused through a monochromator (Jobin Yvon Ltd., UK) and directed to the device under test. A white light bias was used to have similar light intensity conditions to those during normal operation.

Electron lifetime measurements

The measurements were performed with a Dyenamo AB (Sweden) toolbox using a white LED (Luxeon Star 1W) as the light source. Voltage traces were recorded with a 16-bit resolution digital acquisition board (National Instruments); lifetimes were obtained by monitoring photovoltage transients at different light intensities upon applying a small square wave modulation to the base light intensity. The photovoltage response was fitted using first-order kinetics to obtain time constants. The quasi-Fermi level of TiO_2 for the devices was calculated by subtracting the achieved values of V_{OC} from the redox potential of each specific electrolyte.

Electrochemical impedance measurements (EIS)

Impedance measurements were performed using a Bio Logic SP300 potentiostat, over a frequency range from 1 MHz down to 0.1 Hz at bias potentials between 0 and 1.1 V (with a 10 mV sinusoidal AC perturbation). All measurements were done at 20 °C. The resulting impedance spectra were analyzed with Z-view software (v2.8b, Scribner Associates Inc.).

Transient absorption spectroscopy

Nanosecond flash photolysis was used to monitor the microsecond-to-millisecond dynamics. Excitation pulses were generated using a frequency-doubled (532 nm) Q-switched Nd:YAG laser (Continuum Surelite, 20 Hz repetition rate). The excitation fluence for observing charge recombination was attenuated to less than <30 μJ cm^{-2} per pulse, which ideally corresponds to an average of less than 1 electron injected per TiO_2 particle. A continuous wave, cw, Xe arc lamp was used to generate the probe beam. This beam was passed through various filters, a monochromator and multiple lenses before reaching the sample. The resulting probe signal was set at a wavelength of 735 nm and the beam passing through a sample is collected using a second monochromator and delivered to a fast photomultiplier tube (R9910, Hamamatsu) supplied with 750 V, in which the absorption of photons results in electron emission. To obtain a satisfactory signal-to-noise ratio, a digital signal analyser (DPO 7104C, Tektronix) records the induced transient voltage signal, and the data acquisition is averaged over 3000 laser shots, resulting in a sensitivity of 10^{-4} ΔA.

Results and discussion

Cyclic voltammetry was performed to determine the redox potential of AZ and the results are presented in Fig. 1. The redox potentials were referenced at first *vs.* ferrocene/ferrocenium and subsequently *vs.* the standard hydrogen electrode (SHE) by addition of 0.624 V according to the publication by Pavlishchuk and Addison,[28] to obtain a redox potential for the organic donor AZ/AZ^+ of 0.804 V. This redox potential value implies an increase in the difference of the Fermi level of the photoanode and the redox potential, compared to $[Co(bpy)_3]^{3+/2+}$ with a redox potential of 0.56 V *vs.* SHE, and hence, a lower driving force for regeneration is needed. As a result, higher V_{OC} could be reached by using a tandem with Co complexes and AZ. Moreover, the bulkiness of Co complexes provides steric hindrance toward recombination of electrons in the conduction band (CB) of the semiconductor to the redox mediator, which could lead to longer electron lifetimes and enhanced photovoltage and device performance.

A schematic overview of the regeneration reactions in tandem electrolytes containing Co species and AZ is presented in Fig. 2. In principle the photooxidized dye can be regenerated by reacting either with AZ or with $[Co(bpy)_3]^{2+}$. Given the small size of AZ compared to that of the Co complexes, diffusion to the

 This journal is © The Royal Society of Chemistry 2019

Published on 02 April 2019. Downloaded by ECOLE POLYTECHNIC FED DE LAUSANNE on 5/11/2019 11:03:30 AM.

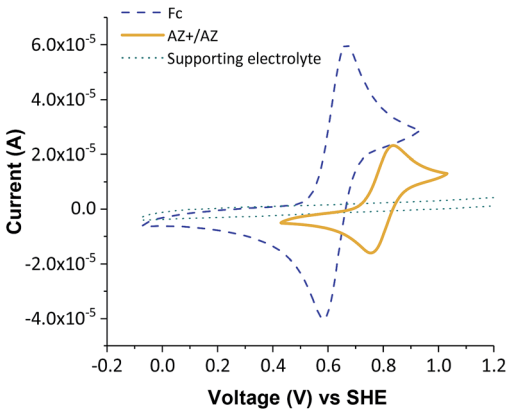

Fig. 1 Cyclic voltammetry with a three-electrode cell with glassy carbon as the working electrode, a graphite rod as the counter electrode, and a non-aqueous reference electrode of Ag/AgCl (2 M in ethanol), and a scan rate of 100 mV s^{-1}.

working electrode of the former can be expected to be rather fast, and it can be reasonably assumed that dye regeneration to a large extent occurs according to eqn (1) than according to the well-known outer-sphere electron transfer from $[Co(bpy)_3]^{2+}$ (eqn (2)). The AZ^+ species thus formed are preferentially reduced to AZ by the Co^{2+} species, with the resulting Co^{3+} species diffusing toward and undergoing reduction at the counter electrode as depicted in the reaction in eqn (3), which at the same time can provide good protection to prevent the recombination reaction of CB electrons with AZ^+.

$$D^+ + AZ \rightarrow D + AZ^+ \quad (1)$$

$$D^+ + [Co(bpy)_3]^{2+} \rightarrow D + [Co(bpy)_3]^{3+} \quad (2)$$

$$AZ^+ + [Co(bpy)_3]^{2+} \rightarrow AZ + [Co(bpy)_3]^{3+} \quad (3)$$

In order to better understand the role of each species in the tandem systems, different compositions were studied: an equimolar ratio of the standard concentration 0.22 M Co(II) and AZ (Co/AZ, 1 : 1), a system with Co(II) in excess (Co/AZ, 1 : 0.8), and a system with AZ in excess (AZ/Co, 1 : 0.9). Electrolyte systems based only on the pair AZ^+/AZ as well as only $[Co(bpy)_3]^{3+/2+}$ were used as reference electrolytes.

Symmetric cells with PEDOT as the CE material and the electrolytes mentioned above were studied. Current *vs.* potential plots with logarithmic current density (log *J*) as a function of voltage (*V*), Fig. 3, were obtained for symmetric cells. The electrochemical parameters are presented in Table 1. The tandem system, AZ/Co 1 : 0.9, exhibits a higher limiting current, J_{lim}, due to the lower concentration of Co(II), the largest ion. In a mixed electrolyte with two redox couples it is not possible to assign a diffusion coefficient to a specific ion. The limiting current, therefore, reflects an overall diffusion of all the ionic species in the mixed electrolyte.

From the sharpness of the curves of the tandem electrolytes it was noted that the addition of AZ to Co-based electrolytes decreased the exchange current, J_0 (intercept at $V = 0$), which can be correlated with the rate of reversible electron-transfer at

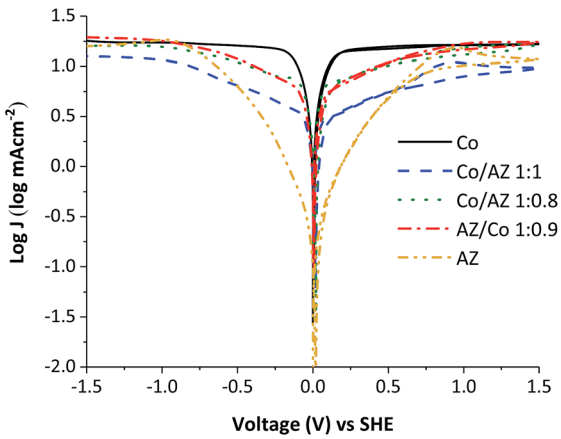

Fig. 3 log(*J*) *vs.* potential plots for symmetrical cells containing tandem electrolytes.

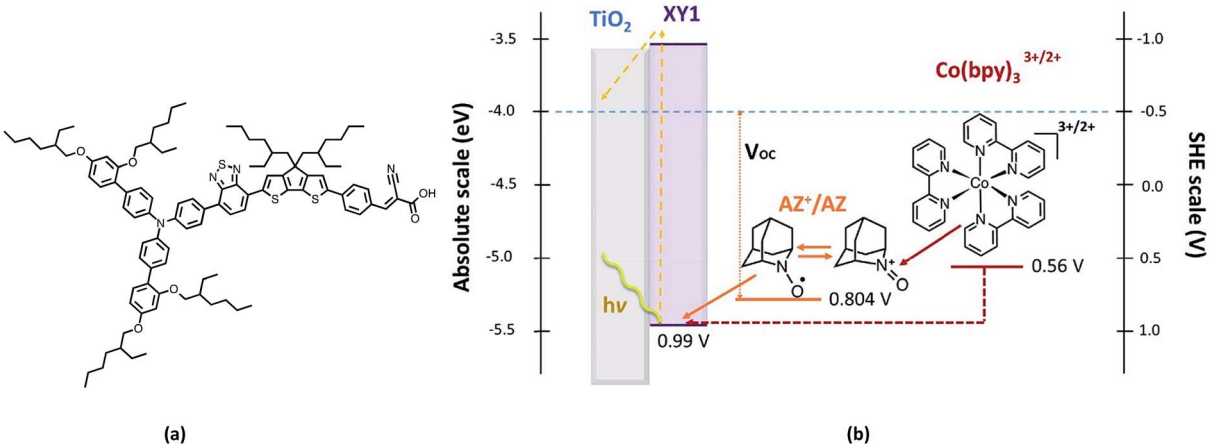

Fig. 2 (a) Chemical structure of the dye XY1 and (b) schematic overview of energetic levels in a DSSC with a tandem electrolyte $[Co(bpy)_3]^{3+/2+}$ + $AZ^{+/0}$; the potentials refer to V *vs.* SHE.

Published on 02 April 2019. Downloaded by ECOLE POLYTECHNIC FED DE LAUSANNE on 5/11/2019 11:03:30 AM.

Table 1 Characterization data of symmetric cells from log(*J*) *vs.* potential plots and from EIS analysis

Electrolyte	J_{lim} (mA cm^{-2})	J_0 (mA cm^{-2})	R_s (Ω cm^{-2})	R_{CT} (Ω cm^{-2})	Z_W (Ω cm^{-2})	D (cm^2 s^{-1})
$[Co(bpy)_3]^{3+/2+}$	16.71	8.87	7.53	0.34	7.14	7.26×10^{-6}
Co/AZ 1 : 1	10.94	4.00	8.82	0.54	24.21	1.39×10^{-5}
Co/AZ 1 : 0.8	16.26	7.17	8.20	0.28	15.09	1.67×10^{-5}
AZ/Co 1 : 0.9	17.51	7.64	7.57	0.69	13.55	1.40×10^{-5}
AZ^+/AZ	15.42	1.12	7.32	81.4	182.6	1.54×10^{-5}

the CE with the reduced species. It was noted that the higher the concentration of AZ, the more pronounced the decrease of the electron transfer rate at the CE, which at the same time can be related to an increase in the charge transfer resistance, R_{CT}, according to eqn (4).[29]

$$J_0 = RF/nR_{CT} \quad (4)$$

EIS spectra were obtained for the symmetric cells and the obtained Nyquist plots, Fig. S5,† were simulated using the equivalent electrical model shown in Fig. S5,† to determine the values corresponding to R_s, which is the series resistance of the symmetric cell, the charge-transfer resistance (R_{CT}) and Z_W the diffusion resistance of all the active species in the electrolyte systems and are presented in Table 1.

The trends observed from the electrochemical measurements follow the same tendency as the fitted values from the EIS measurements, where among the three different tandem electrolytes, the system with AZ/Co 1 : 0.9 presented the lowest value of Nernst diffusion impedance, Z_W in the electrolyte. This can be correlated with a lower resistance to the diffusion of the ionic species in the mixed electrolyte, leading to higher diffusion coefficients.

The diffusion coefficients for all the electrolytes were measured with a rotating disk electrode and are presented in Table 1. The obtained value for the $Co(bpy)_3^{2+}$ species was 7.26 $\times 10^{-6}$ cm^2 s^{-1} which is in accordance with the values reported by several authors.[30–34] The AZ^0 species in the AZ^+/AZ electrolyte showed a diffusion coefficient of 1.58 $\times 10^{-5}$ cm^2 s^{-1}, in agreement as expected from its smaller size compared to the cobalt complexes. It is important to denote that the diffusion coefficients of the tandem electrolytes presented in Table 1 account for the overall diffusion of the species Co^{2+} and AZ into each mixture, and it was not possible to assign the contribution of each species to the total limiting current (Fig. S4†). Nonetheless, it is interesting to note that by forming tandem electrolytes, the diffusion coefficients remained similar to that of the AZ^+/AZ electrolyte. Furthermore, we were able to determine the diffusion coefficient of the AZ^+ species (Table S.1†) in the AZ^+/AZ electrolyte to be 1.87 $\times 10^{-7}$ cm^2 s^{-1}, which explains the high R_{CT} found for the symmetrical cells for the AZ^+/AZ electrolyte.

Subsequently, complete devices were tested using the dye XY1 (Fig. 2(a)) and PEDOT as the CE material, and the *J*–*V* curves are shown in Fig. 4(a).

As observed, the devices containing the electrolytes Co(II)/AZ 1 : 08 and AZ/Co 1 : 0.9 presented a significant improvement in the overall performance compared to the cobalt reference electrolyte in complete devices, which indicates the advantage of using tandem electrolyte-systems.

The AZ^+/AZ electrolyte displayed high conversion efficiency at low light intensities, around 8.2% at 0.1 sun (Table S.1†); however the non-linearity observed for the AZ^+/AZ electrolyte from Fig. 4(b) can be explained by the irreversibility of AZ at the CE since the AZ^+ species cannot reach the CE fast enough due to its low diffusion coefficient. The AZ molecules can reach the photoanode rapidly to regenerate the dye, but are not effectively reduced at the CE, decreasing the concentration

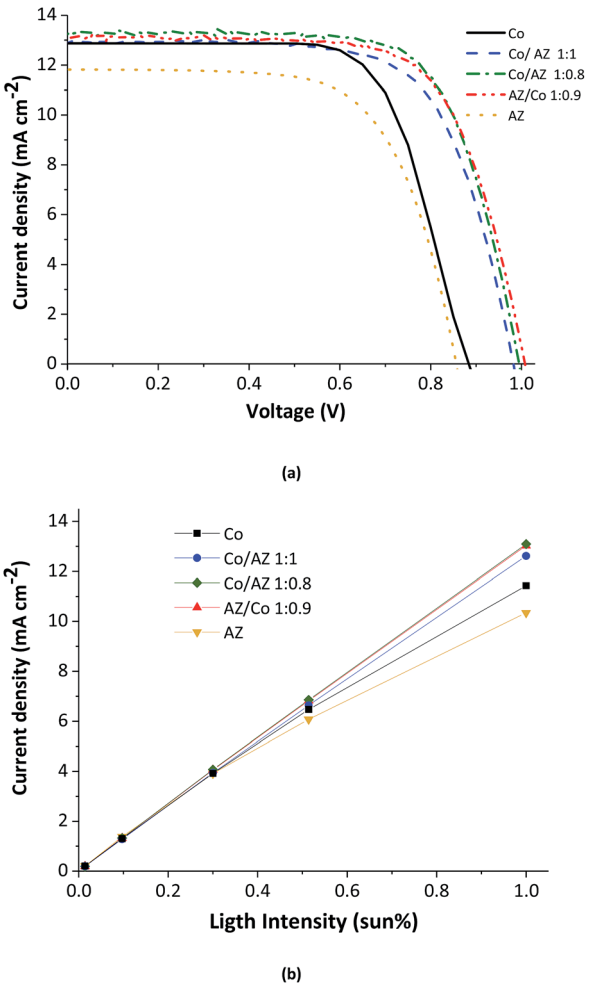

Fig. 4 (a) *J*–*V* curves for DSSCs with tandem system electrolytes and (b) light intensity–current dependence.

 This journal is © The Royal Society of Chemistry 2019

Published on 02 April 2019. Downloaded by ECOLE POLYTECHNIC FED DE LAUSANNE on 5/11/2019 11:03:30 AM.

of AZ in the electrolyte affecting the dye regeneration rate. Additionally, the FF drastically decreased with the increase of light intensity. The same trend was observed for the tandem system Co/AZ 1 : 1, which indicates that high concentrations of AZ increase the charge transfer resistance at the CE due to the aforementioned irreversibility of AZ at the PEDOT CE.

In contrast, it can be observed from Fig. 4(b) that the addition of lower concentrations of AZ in the tandem electrolytes improved the linearity of the current density as a function of light intensity, opposed to the Co-reference electrolyte, being hampered by mass-diffusion limitations due to the large size of the complexes. This could indicate that the small AZ molecules reach the electrodes faster than the bulky cobalt species, increasing the dye regeneration rate. However, the oxidized species of AZ^+ are reduced by Co^{2+} fast enough as stated in eqn (3), instead of being reduced at the CE, where the produced Co^{3+} species can be effectively reduced to Co^{2+}.

The highest J_{SC} was obtained for the Co/AZ 1 : 0.8 system, which can be explained by a faster dye regeneration rate which results in a faster injection rate. Additionally, for the tandem system with an excess of AZ and a low concentration of Co(II) (AZ/Co 1 : 0.9) a higher photovoltage exceeding 1 V was obtained. This could indicate that AZ plays a major role in the determination of the V_{OC} of the cell as previously discussed.

The highest IPCE was obtained for the Co/AZ 1 : 0.8 tandem system, which agrees with J_{SC} from the J–V curves. Additionally, the IPCE depends on the light harvesting efficiency, η_{LH}, electron injection efficiency, η_{inj}, and charge collection efficiency, η_{cc}, as in eqn (5).

$$\mathrm{IPCE} = \eta_{LH}(\lambda)\eta_{inj}(\lambda)\eta_{cc}(\lambda) \quad (5)$$

Given the high molar extinction coefficient for the dye XY1, η_{LH} is close to 100% at the maximum light absorbance (absorbance = P(abs)/P(in)), corrected for reflection losses. Therefore η_{LH} should not be the limiting factor for the differences observed in Fig. 5. The electron injection efficiency from the excited sensitizer into the TiO_2 conduction band (CB) and collection efficiency are both expected to greatly affect the IPCE in tandem electrolytes. A faster and more efficient regeneration of the dye molecules can be expected with the tandem systems, increasing η_{inj}. At the same time, a much faster dye regeneration than recombination between conduction band electrons and oxidized dye molecules will increase η_{cc} since it will interrupt the recombination.

The V_{OC} for a complete device under illumination is the result of the difference of the quasi Fermi level, $E_{F,q}$, of the TiO_2 and the Nernst potential of the redox couple in the electrolyte, the former being determined by the position of the conduction band of TiO_2 and the rate of recombination of photogenerated electrons from the conduction band to the electrolyte.

The differences in V_{OC} observed for the tandem electrolytes were studied by charge extraction and V_{OC} decay measurements as a function of light intensity (transient measurements) and the results are displayed in Fig. 6 as a function of $E_{F,q}$.

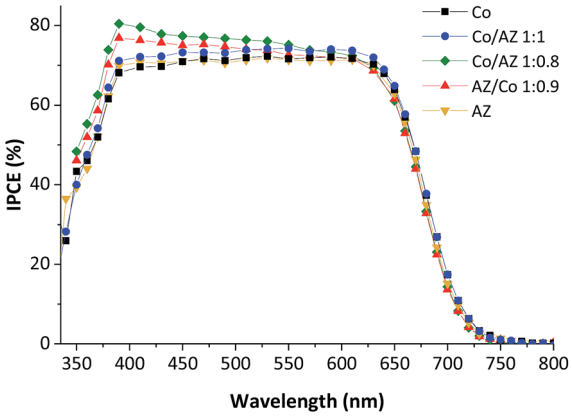

Fig. 5 IPCE curves for the tandem systems.

The quasi-Fermi level for devices with the $[Co(bpy)_3]^{3+/2+}$ electrolyte and for the AZ^+/AZ was obtained using the relationship $E_{F-q} = E_{redox} - V_{OC}$.[35] An approximation of the E_{redox} of each tandem system was estimated by the average of the E_{redox} of $[Co(bpy)_3]^{3+/2+}$ and AZ^+/AZ in each electrolyte. This approximation was supported by a chronopotentiometry method at zero current, Fig S3.† From these measurements, the open circuit voltage of a tandem electrolyte with 2 mM $[Co(bpy)_3]^{2+}$, 0.5 mM $[Co(bpy)_3]^{3+}$, 0.1 M LiTFSI, 2 mM AZ and 0.1 mM AZ^+ by adding the corresponding amount of $NOBF_4$ was around 0.62 V. On a working device under illumination, the concentration of AZ^+ is rather uncertain; however Co^{2+} species can reduce AZ^+ fast enough, and the concentration of AZ^+ in the electrolyte can be reasonably expected to be low. Thus, the average of the E_{redox} of both redox pairs is a good approximation to estimate the quasi-Fermi level of devices with tandem electrolytes.

Therefore, in Fig. 6(a), the charge extraction is depicted *vs.* the quasi-Fermi level of the electrons in the TiO_2 conduction band under illumination for complete devices. A downward-shift compared to the $[Co(bpy)_3]^{3+/2+}$ electrolyte as a reference was observed for all the electrolytes containing AZ^0. This effect could be attributed to adsorption of the AZ^+ cations onto the TiO_2 layer, which are neutralized by electrons from the CB, consequently shifting down the Fermi level of TiO_2. Nonetheless, this effect does not represent a dramatic loss in V_{OC} since for all the tandem systems the CB edge still lies at values above 0 V *vs.* SHE.

It is interesting to note from Table 2 that the devices with the AZ^+/AZ electrolyte reached a V_{OC} of 856 mV, which is similar to the V_{OC} obtained using the $[Co(bpy)_3]^{3+/2+}$ reference, although it has a redox potential 0.24 V lower than AZ^+/AZ. The reason for this similarity can be explained by the combined result of the positive shift of the quasi-Fermi level of TiO_2 for the for AZ^+/AZ electrolyte and the higher electron lifetime for $[Co(bpy)_3]^{3+/2+}$ electrolyte.

Moreover, it is significant to note from Fig. 6(b) that all the tandem electrolytes presented longer electron lifetimes compared to the $Co^{3+/2+}$ electrolyte, which indicates an even

Published on 02 April 2019. Downloaded by ECOLE POLYTECHNIC FED DE LAUSANNE on 5/11/2019 11:03:30 AM.

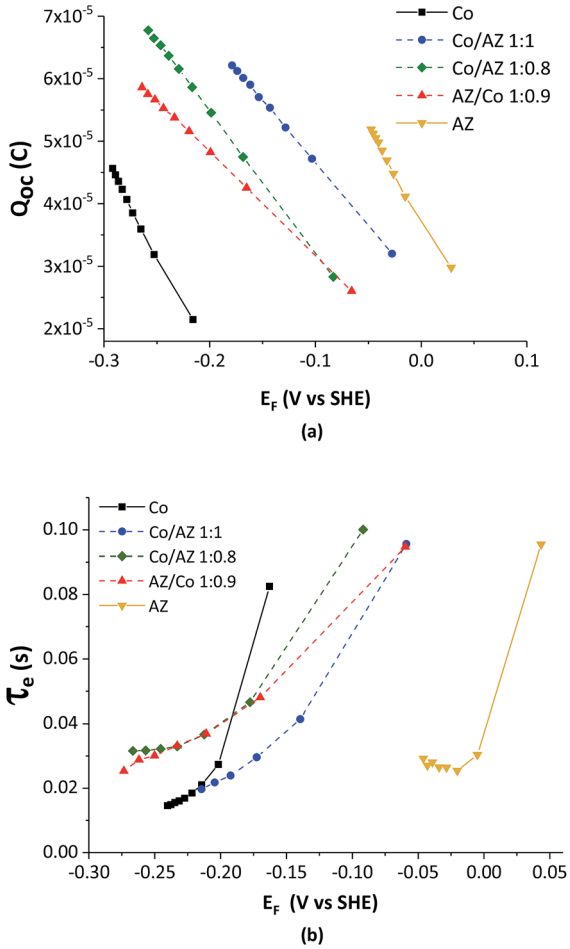

Fig. 6 (a) Charge extraction *vs.* Fermi level and (b) electron lifetime *vs.* Fermi level of DSSCs containing tandem electrolyte systems. For both plots, the squares correspond to the $[Co(bpy)_3]^{3+/2+}$ reference, the circles to Co/AZ 1 : 1, diamonds to Co/AZ 1 : 0.8, triangles to AZ/Co 1 : 0.9 and inverted triangles to the $AZ^{+/0}$ electrolyte. The quasi-Fermi level was obtained using the relationship $E_{F-q} = E_{redox} - V_{OC}$, and the E_{redox} of the tandem systems was approximated from the average of the E_{redox} of $[Co(bpy)_3]^{3+/2+}$ and AZ^+/AZ.

Table 2 Characteristic *I*–*V* parameters for the tandem electrolyte systems at 1 sun intensity

Electrolyte	V_{OC} (mV)	J_{SC} (mA cm^{-2})	FF	η (%)
$[Co(bpy)_3]^{3+/2+}$	896	12.87	0.69	7.96
Co/AZ 1 : 1	982	12.89	0.68	8.52
Co/AZ 1 : 0.8	995	13.23	0.71	9.15
AZ/Co 1 : 0.9	1008	13.16	0.69	8.97
AZ^+/AZ	856	11.82	0.66	6.67

lower recombination rate for this system, explaining the higher V_{OC} (exceeding 1 V) obtained for the tandem electrolytes.

On the other hand, the down-shift of the quasi Fermi level observed from Fig. 6(a) implies a larger driving force for electron injection from the LUMO of the dye to the CB of the TiO_2; consequently faster electron injection for these systems can explain the differences observed in the IPCE measurements due to the improved η_{inj}.

To better understand the changes in the V_{OC} of the devices, EIS analysis on complete devices in the dark was performed. The obtained Nyquist plots (Fig. S6†) were fitted according to the transmission-line model developed by Bisquert *et al.*,[36] where, R_{CT}, refers to the recombination resistance for the electrons in the TiO_2 conduction band with the oxidized form of the redox couple, the chemical capacitance, C_μ, is related to the density of states (DOS) accessible to electrons in the TiO_2, and the transport resistance, R_{trans}, is related to the hindrance caused by the TiO_2 network to the transport of electrons through the film. The most relevant results from the EIS fitting are presented in Fig. 7.

The observed trends for electron recombination and electron lifetimes under dark conditions are in accordance with the behaviour under illumination, Fig. 7(b), where the tandem

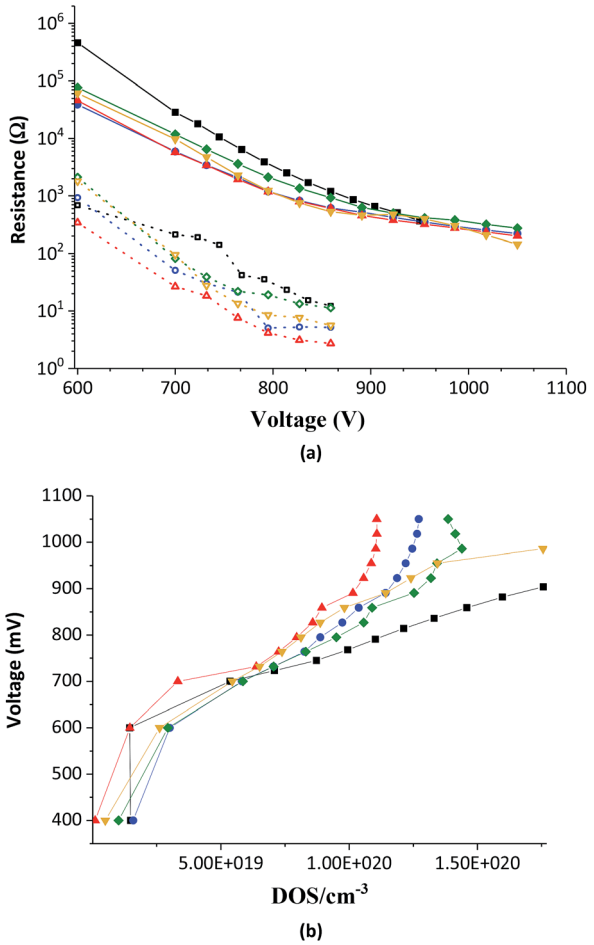

Fig. 7 EIS analysis. (a) Continuous lines with solid markers represent the charge transfer resistance R_{CT} as a function of applied voltage and the dotted lines with open markers represent the transport resistance R_{trans}. (b) Voltage *vs.* DOS/cm^{-3}. The squares correspond to the $[Co(bpy)_3]^{3+/2+}$ reference, the circles to Co/AZ 1 : 1, diamonds to Co/AZ 1 : 0.8, triangles to AZ/Co 1 : 0.9 and inverted triangles to the $AZ^{0/+}$ electrolyte.

This journal is © The Royal Society of Chemistry 2019

Published on 02 April 2019. Downloaded by ECOLE POLYTECHNIC FED DE LAUSANNE on 5/11/2019 11:03:30 AM.

systems presented higher recombination resistance and higher electron lifetimes than the $[Co(bpy)_3]^{3+/2+}$ reference.

The most important differences between the devices with different electrolytes are shown in the region of high forward bias, Fig. 7(a), where the system Co/AZ 1 : 0.8 presents higher R_{CT} compared to the cobalt reference, in particular from 900 mV to higher voltages, as well as smaller R_{trans} (higher electron lifetime), improving the electron collection efficiency. This explains why, under the employed conditions, the highest performance in the *J–V* measurements was obtained for this electrolyte due to a higher J_{SC}, and better R_{CT} and R_{trans}.

The position of the conduction-band edge of devices containing the tandem electrolytes under dark conditions, Fig. 7(b), are in agreement with the trends observed from the charge extraction measurements under illumination. A down-shift of the CB edge was observed for all the devices containing AZ compared to the cobalt reference electrolyte, since the latter presents higher electron occupancy from 750 mV to 900 mV, which can be related to a higher quasi-Fermi level. The shift in the quasi-Fermi level for the tandem systems can be attributed to adsorption of the AZ^+ cations onto the TiO_2 layer. It can also be noted that the displacement of the Fermi level is less significant in the dark than under light conditions.

Under illumination, dye regeneration by AZ increases the concentration of AZ^+, which further displaces the Fermi level to more negative values in the SHE scale. The higher concentration of AZ^+ both in the tandem system Co/AZ 1 : 1 and in the devices with the AZ^+/AZ electrolyte lead to a higher displacement as observed from Fig. 6.

The clear effect of using AZ as a small donor in the tandem electrolytes is reflected on the dye regeneration rate obtained from transient absorption spectroscopy measurements (Fig. 8). The regeneration half-times obtained from the decay-plot fitting are presented in Table 3.

As expected due to the its small size, the AZ^+/AZ electrolyte presents a faster regeneration rate than the cobalt reference; however all the tandem systems presented even faster regeneration rates than the AZ^+/AZ electrolyte; this could be attributed to efficient reduction of the AZ^+ molecules by Co^{2+}.

The tandem system Co/AZ 1 : 0.8 is slightly faster than the tandem with an excess of AZ (AZ/Co (1 : 0.9)), which explains the difference in J_{SC} obtained for this system.

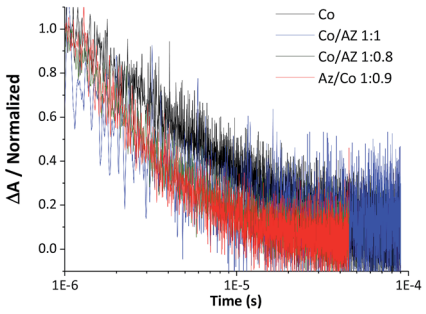

Fig. 8 Transient absorption spectroscopy measurements of DSSCs with tandem electrolytes.

Table 3 Regeneration halftimes obtained from transient absorption spectroscopy measurements

Electrolyte	τ_{reg} (μs)	η_{reg} (%)
$[Co(bpy)_3]^{3+/2+}$ ref.	6.29	99.22
Co/AZ (1 : 1)	2.81	99.65
Co/AZ (1 : 0.8)	2.13	99.73
AZ/Co (1 : 0.9)	2.45	99.69
AZ 0.25 M	3.58	99.56
Inert, ACN	0.81 ms (τ_{rec})	—

Conclusions

We studied the behavior of tandem electrolytes containing two redox species (as well as commonly used additives) in liquid media, the organic radical 2-azaadamantane-*N*-oxyl with the corresponding form (AZ^0/AZ^+) and the well-known redox pair $[Co(bpy)_3]^{2+/3+}$. DSSCs fabricated with this electrolyte reached V_{OC} values up to 1007 mV and had higher performance than DSSC devices with either of the component redox mediator electrolytes in conjunction with the panchromatic dye XY1. It was determined that the V_{OC} improvement is due to two main factors, the more positive redox potential of the $AZ^{+/0}$ redox couple and the lower recombination rates of the electrons from the CB to the electrolyte. From studying different composition systems, an optimal concentration for AZ^0/AZ^+ was obtained. It was determined that high concentrations of AZ decrease the fill factor and may also result in the adsorption of AZ^+ molecules on the oxide surface. These results demonstrate the advantages of using tandem electrolytes containing two redox mediators and indicate that future work could further improve the V_{OC} and overall performance of DSSCs as well as the long-term stability of the devices.

Conflicts of interest

There are no conflicts to declare.

Acknowledgements

We acknowledge the Swiss National Science Foundation for financial support with the project entitled as “Fundamental studies of dye-sensitized and perovskite solar cells” with project number 200020_169695.

References

1 B. O'Reagan and M. Grätzel, *Nature*, 1991, **353**, 737–740.
2 K. Kakiage, Y. Aoyama, T. Yano, K. Oya, J. Fujisawa and M. Hanaya, *Chem. Commun.*, 2015, **51**, 15894–15897.
3 K. Kalyanasundaram, A. Hagfeldt, G. Boschloo, L. Sun, L. Kloo and H. Pettersson, *Chem. Rev.*, 2010, **110**, 6595–6663.
4 J. Bisquert, *J. Phys. Chem. C*, 2007, **111**, 17163–17168.
5 J. Teuscher, A. Marchioro, J. Andrès, L. M. Roch, M. Xu, S. M. Zakeeruddin, P. Wang, M. Grätzel and J. E. Moser, *J. Phys. Chem. C*, 2014, **118**, 17108–17115.

Published on 02 April 2019. Downloaded by ECOLE POLYTECHNIC FED DE LAUSANNE on 5/11/2019 11:03:30 AM.

6 G. Boschloo and A. Hagfeldt, *Acc. Chem. Res.*, 2009, **42**, 1819–1826.
7 S. Ito, P. Liska, P. Comte, R. Charvet, P. Péchy, U. Bach, L. Schmidt-Mende, S. M. Zakeeruddin, A. Kay, M. K. Nazeeruddin and M. Grätzel, *Chem. Commun.*, 2005, 4351–4353.
8 Z. Sun, M. Liang and J. Chen, *Acc. Chem. Res.*, 2015, **48**, 1541–1550.
9 J.-H. Yum, E. Baranoff, F. Kessler, T. Moehl, S. Ahmad, T. Bessho, A. Marchioro, E. Ghadiri, J.-E. Moser, C. Yi, M. K. Nazeeruddin and M. Grätzel, *Nat. Commun.*, 2012, **3**, 631.
10 T. Moehl, H. N. Tsao, K. L. Wu, H. C. Hsu, Y. Chi, E. Ronca, F. De Angelis, M. K. Nazeeruddin and M. Grätzel, *Chem. Mater.*, 2013, **25**, 4497–4502.
11 S. Mathew, A. Yella, P. Gao, R. Humphry-Baker, B. F. E. Curchod, N. Ashari-Astani, I. Tavernelli, U. Rothlisberger, M. K. Nazeeruddin and M. Grätzel, *Nat. Chem.*, 2014, **6**, 242–247.
12 M. Safdari, P. W. Lohse, L. Häggman, S. Frykstrand, D. Högberg, M. Rutland, R. Álvarez, J. Gardner, L. Kloo, A. Hagfeldt and G. Boschloo, *RSC Adv.*, 2016, **6**, 56580–56588.
13 A. Yella, H.-W. Lee, H. N. Tsao, C. Yi, A. K. Chandiran, M. K. M. K. Nazeeruddin, E. W.-G. Diau, C.-Y. Yeh, S. M. Zakeeruddin, M. Grätzel, M. Gratzel and M. Grätzel, *Science*, 2011, **334**, 629–634.
14 Y. Liu, J. R. Jennings, Y. Huang, Q. Wang, S. M. Zakeeruddin and M. Grätze, *J. Phys. Chem. C*, 2011, **115**, 18847–18855.
15 S. Aghazada, P. Gao, A. Yella, G. Marotta, T. Moehl, J. Teuscher, J.-E. E. Moser, F. De Angelis, M. Grätzel and M. K. Nazeeruddin, *Inorg. Chem.*, 2016, **55**, 6653–6659.
16 M. Wang, N. Chamberland, L. Breau, J.-E. Moser, R. Humphry-Baker, B. Marsan, S. M. Zakeeruddin and M. Grätzel, *Nat. Chem.*, 2010, **2**, 385–389.
17 M. Freitag, Q. Daniel, M. Pazoki, K. Sveinbjörnsson, J. Zhang, L. Sun, A. Hagfeldt and G. Boschloo, *Energy Environ. Sci.*, 2015, **8**, 2634–2637.
18 Y. Cao, Y. Liu, S. M. Zakeeruddin, A. Hagfeldt and M. Grätzel, *Joule*, 2018, **2**, 1108–1117.
19 Y. Cao, Y. Saygili, A. Ummadisingu, J. Teuscher, J. Luo, N. Pellet, F. Giordano, S. M. Zakeeruddin, J.-E. Moser, M. Freitag, A. Hagfeldt and M. Grätzel, *Nat. Commun.*, 2017, **8**, 15390.
20 F. Kato, N. Hayashi, T. Murakami, C. Okumura, K. Oyaizu and H. Nishide, *Chem. Lett.*, 2010, **39**, 464–465.
21 W. Yang, N. Vlachopoulos, Y. Hao, A. Hagfeldt and G. Boschloo, *Phys. Chem. Chem. Phys.*, 2015, **17**, 15868–15875.
22 C. T. Li, C. P. Lee, C. T. Lee, S. R. Li, S. S. Sun and K. C. Ho, *ChemSusChem*, 2015, **8**, 1244–1253.
23 J. Cong, Y. Hao, G. Boschloo and L. Kloo, *ChemSusChem*, 2015, **8**, 264–268.
24 Y. Hao, W. Yang, L. Zhang, R. Jiang, E. Mijangos, Y. Saygili, L. Hammarström, A. Hagfeldt and G. Boschloo, *Nat. Commun.*, 2016, **7**, 13934.
25 W. Yang, M. Söderberg, A. I. K. Eriksson and G. Boschloo, *RSC Adv.*, 2015, **5**, 26706–26709.
26 F. Kato, A. Kikuchi, T. Okuyama, K. Oyaizu and H. Nishide, *Angew. Chem.*, 2012, **124**, 10324–10327.
27 M. Shibuya, M. Tomizawa, I. Suzuki and Y. Iwabuchi, *J. Am. Chem. Soc.*, 2006, **128**, 8412–8413.
28 V. V. Pavlishchuk and A. W. Addison, *Inorg. Chim. Acta*, 2000, **298**, 97–102.
29 M. Chen, L. Shao, Y. Xia, Z.-Y. Huang, D.-L. Xu, Z.-W. Zhang, Z.-X. Chang and W.-J. Pei, *ACS Appl. Mater. Interfaces*, 2016, **8**, 26030–26040.
30 S. M. Feldt, P. W. Lohse, F. Kessler, M. K. Nazeeruddin, M. Grätzel, G. Boschloo and A. Hagfeldt, *Phys. Chem. Chem. Phys.*, 2013, **15**, 7087.
31 S. M. Feldt, G. Wang, G. Boschloo and A. Hagfeldt, *J. Phys. Chem. C*, 2011, **115**, 21500–21507.
32 M. Freitag, F. Giordano, W. Yang, M. Pazoki, Y. Hao, B. Zietz, M. Grätzel, A. Hagfeldt and G. Boschloo, *J. Phys. Chem. C*, 2016, **120**, 9595–9603.
33 L. Kavan, J.-H. Yum and M. Grätzel, *Nano Lett.*, 2011, **11**, 5501–5506.
34 S. M. Feldt, E. a Gibson, E. Gabrielsson, L. Sun, G. Boschloo and A. Hagfeldt, *J. Am. Chem. Soc.*, 2010, **132**, 16714–16724.
35 W. Yang, N. Vlachopoulos, Y. Hao, A. Hagfeldt and G. Boschloo, *Phys. Chem. Chem. Phys.*, 2015, **17**, 15868–15875.
36 F. Fabregat-Santiago, G. Garcia-Belmonte, I. Mora-Seró and J. Bisquert, *Phys. Chem. Chem. Phys.*, 2011, **13**, 9083.

 This journal is © The Royal Society of Chemistry 2019